Journal of Mechanical Engineering Research and Developments
ISSN: 1024-1752
CODEN: JERDFO
Vol. 44, No. 3, pp. 138-150
Published Year 2021

Numerical Investigations of Fluid Structural Interaction for Aircraft Wing Flap Structure Using CFD Technique

Ali Al-Zughaibi, Emad Q. Hussein, Farhan Lafta Rashid

College of Engineering, University of Kerbala-Iraq

*Corresponding Author Email: emad.dujaily@uokerbala.edu.iq

ABSTRACT: Fluid-structure interaction plays a vital role and influences system design. The purpose of this paper is to present a robust strategy of investigating the effect of flap geometry on structure analysis of NACA 23012 airfoiled flying wing. The proposed model has been tested with three configurations, 20% C, 30% C and 40% C of the single plain flap at an effective specific Reynold's number (Re) beneath subsonic fluid flow condition. The simulated model has been solved the governing equations such as: Continuity, Reynolds Averaging Never-Stokes, and Energy Equation. Thus, in cooperative with analysis of dynamic meshing technique to predict the wing pressure distribution through variation of flap angles and setting Angle of Attack (AoA). The induced equivalent von- Mises stress and the total deformation according to the flow has been successfully computed using the ANSYS program. As a result, the stress and deformation increment highly relative to a larger flap chord. The maximum value of stress is 40% greater than others, while the maximum deflection is 45%, thus, it should be considered within wing design. It is eventually seen that the average pressure distribution over airfoil increases relative to growth in the flap angle for all cases. The maximum value of average pressure was found at the flap angle approximated to 5°. The maximum value of stress (100.03 MPa) was found at the root of the wing relative to the maximum bending moment occurs at the root. So, the maximum deflection occurs at the free side of the tip wing at (301.35 mm). The comparison of the pressure coefficient with the previous measurement is performed to prove the effectiveness and reality of the CFD simulates model.

KEYWORDS: Angle of Attack, dynamic mesh, flap angle, fluid structure, subsonic flow.

INTRODUCTION

A class of problems with mutual dependence between the fluid-structure and structural mechanics parts is Fluid-Structure Interaction (FSI). Physics and aerodynamics students are taught that airplanes fly as a result of Bernouli's principle, they said that if the airspeed grows up the pressure is dropped. A wing produces lift which is due to air goes faster over the top creating of the low-pressure region. Some interested people may ask: why the air moves faster over the top surface of the wing? [1].

If an external force act on the airplane, such as normal airflow over the surfaces, thus lead to creating very-low-level vibrations. Instruments of high lift have a great impact on the performance of operating cost aircraft, specifically through the landing stage and take-off. In addition, the devices of high lift mechanical system has a great relation with design cost and airplane weight. An improved version of the flap is slotted flap, producing high lift as mentioned by Juan F. Granizo [2]. The airflow when full flaps are deployed creates a maximum lift which helps to move the boundary layer farther forward, near the center of the chord, of the lower surface of the wing. This airflow changing hits the open landing gear wheel will create subtle buffeting that passengers feel. This is particularly true if passengers seated directly over the wing, where the fuselage connects to the wing spars. The important part that prevent the early separation is the slot, so the flap remain effective for angles of larger deflection [3].

The two methods used to determine the fluid-structure interaction effects in the time domain were governing equations in such strongly or partially coupled. In the fully coupled mode, the flow filed, and the structure responds simultaneously found through alternating the aerodynamic forces and the structural displacement. In this process, the structure and fluid analysis equations are integrated together in the form of a combined set of equations, then it is solved and incorporated simultaneously all the variables including the interface of fluid-structure [4]. In the full potential equations or transonic small disturbance equations, panel method were frequently used to compute the aerodynamic loads among the aeroelastic problems. The small disturbance transonic equations are suitable for the flows at a small AOA (Angle of Attack) only. The full potential equations tend to abandonment both swirl

and viscosity [5]. In the partly coupled model, the response of structural lags the solution of flow field. This process deals the structure and fluid as two separate modules with updating the Computational Fluid Dynamics (CFD) and the Computational Structural Dynamics (CSD), which was separately variable with a transfer adjustable at the interface of fluid-structure. This procedure is widely applied because it the codes of CFD and the Finite Element Method (FEM) by interpolating both the structural nodes and the aerodynamic nodes [6,7].
This study is focused on the investigation of NACA 23012 airfoil in 3D with different flap geometry, through properly simulated the flow over the airfoil equipped with movable flap at setting AoA. The wing was considered to be rigid; this allows to obtain the pressure distribution over it. This load distribution was transferred to the structure analysis, which incorporates to determine wing stress and deformation.

PHYSICAL MODEL

In this work, the flow filed around airfoil has been studied and the geometry of the bodies has been simplified within the numerical model. The NACA 23012 airfoil with different flap length as presented in Fig. 1, is with the 2% C slotted flap gap in all cases, whose length of flap is expressed as percentages of the airfoil chord. The airfoil will be modelled with varies flap angles at a set AoA [8].

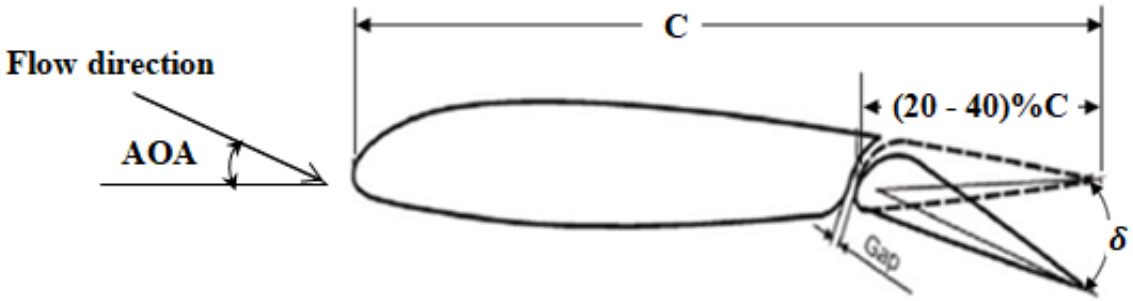

Figure 1. Physical model of 23012 airfoil with single slotted flap

METHODOLOGY

In this study, 3D numerical simulations were performed by the Fluent software.The fluid and structural domain may be solved without any modification in their respective by using explicit method. System of structural analysis is joined with CFD using Ansys 17.2 to perform coupled simulations with transfer all data. The physics of fluid and structural field are solved individually and then collected using Fluid-Solid Interface (FSI). The simulation of FSI used the same geometrical model as it used in the simulation of Fluent. The equations in the ALE(Arbitrary Lagrangian Eulerian) differential form can be obtained from the equation of mass, moment and energy[9,10].

$$\frac{d\rho}{dt} = \frac{\partial \rho}{\partial t} + v.\nabla\rho = -\rho\nabla.v \ , \qquad \text{mass}$$

$$\frac{dv}{dt} = \rho\left\{\frac{\partial v}{\partial t} + (v.\nabla)v\right\} = \nabla.\sigma + \rho b \ , \qquad \text{momentum}$$

$$\frac{dE}{dt} = \rho\left\{\frac{\partial E}{\partial t} + v.\nabla E\right\} = \nabla.(\sigma.v) + v.\rho b \ , \qquad \text{energy}$$

Where, ρ is the density, σ the Cauchy stress tensor, v the material velocity, E the specific total energy and , b the specific body force.

The governing equations of the structure will be stated brifly in the following sections. The problems consist of a fluid which is occupied a specified domain which interact at the well-defined boundary Γ. The possibly large displacement of the structure is governed by:

$$\rho^S \frac{D^2u}{Dt^2} - \nabla.\big(F.S(u)\big) = \rho^S b^S \qquad in\ \omega^S \times (0,T)$$

Where b^S is the body forces applied on the structure, u is the displacements of the structure. ρ^S is the density of the structure, S is the second Piola-Kirchhoff stress tensor, and F is the deformation gradient tensor. All equations of fluid which are the incompressible Navier-Stokes equations wrote in ALE formula [11].

$$\rho^F \frac{dv}{dt}\Big|_\chi + \rho^F . c. \nabla v - 2\mu \nabla . \epsilon(v) + \nabla \bar{P} = \rho^F b^F \qquad in\ \omega^F \times (0, T)$$

Where, $\boldsymbol{v}$ represents the velocity of fluid and $\bar{P}$ represents the physical pressure. The fluid density and viscosity is given as ρ^F and μ, respectively. $\epsilon(v)$ denotes to the tensor of strain rate.

Coupling equations

At the interface Γ , dynamic and kinematic continuity is needed. The equations of governing kinematic coupling are[9]:

$$u_\Gamma(t) = d_\Gamma^F(t)$$
$$\dot{u}_\Gamma(t) = v_\Gamma(t)$$
$$\ddot{u}_\Gamma(t) = \dot{v}_\Gamma(t)$$

Where, d_Γ denotes the fluid mesh nodes displacement at the interface.

PROBLEM SPECIFICATION

In an external flow such as that over an wing with flap, it was vital to define a far-field boundary and the mesh of the region between the body geometry and boundary. The geometric model consists of a domain with radius 10 times length of the airfoil, which is located in the middle of the domain as conducted by many researchers [12, 13, 14], as shown in Fig. 2. A grid indepdence study was carried out to determine how the used mesh is suitable for accurate results and computing time during analysis, the goodness of the computational regions will play an important role in the stability and accuracy of the analysis. Consequently, to control the quality of the mesh, several criteria can be used to estimate the Fluent such as maximum cell skewness and maximum aspect ratio. The degree of accuracy was identified the mesh resolution, it was greater in the domain, for example, the region closes to the body geometry**.**The final process of meshing is to define the boundary condition for the model.

After the meshing of the model was completed, it was applying Ansys Fluent 17.2 and the parameter for the simulation was established. A pressure far-field boundary condition allows the user to specify Mach number, static pressure, static temperature and turbulent condition for the flow at the free stream flow locations. The methodology was based on the solver pressure based on the viscous model as Spalart-Allmaras. The air density can be evaluated using the ideal gas law, while Sutherland's was used to estimate the air viscosity in a similar approach.

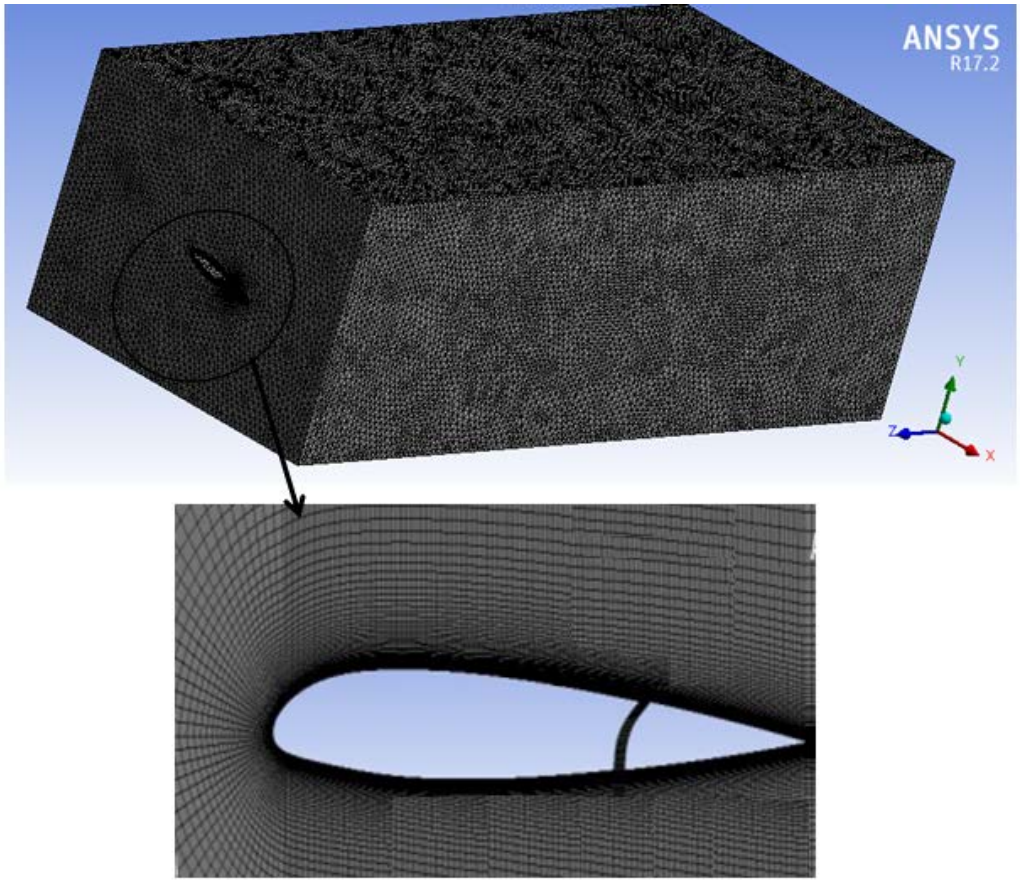

Figure 2. Mesh generation of the wing NACA23012 in 3D.

DYNAMIC MESH

The dynamic mesh capability is used to transient a wing with flap simulation problems with boundary motion. The requirements of the dynamic simulation are an initial mesh and description of the boundary motion. In the current study, the defection of the flap is described by a User Define Function (UDF), the detail of considering UDF were demonstrated in such research [15]. A UDF is a function defined by the C-programming language scheme, which can be dynamically linked with the Fluent as a compiled function. The travel of the moving wall (flap) described employing UDF within using the dynamic mesh model. The UDF code defines the mesh motion through dynamic zones, which corresponds to the center of gravity motion of wing with flap. The spring-based smoothing was used to update the mesh volume in the deforming zones.

VALIDATION OF THE RESULTS

The results of previous tests of a NACA 23012 airfoil with a slotted flap (20% C) at a setting of AoA, are compared with the current results. In this study, the diagram of pressure coefficient over the surface is obtained as the ratio of the static pressure, as shown in Fig.3, which covered a point on the airfoil to the free stream dynamic pressure at zero angles of the flap and AoA settings equal to 12°.The validation of pressure coefficient between CFD simulation and experimental results at ($Re=3*10^{6}$) under subsonic fluid flow, is illustrated in Fig.4, and this totally agreement with other studies [16, 17]. As a result, the CFD modelling and simulating method used in this study have been successfully predicted the flow around the wing, when the flow is attached. This comparison identified, the NACA 23012 airfoil was generally slightly higher than the present test. The percentage maximum difference in the pressure coefficient was obtained from the validation of the airfoil is less than 12%. The error is mostly related to the boundary layers treatment and can be overcome only by a transient.

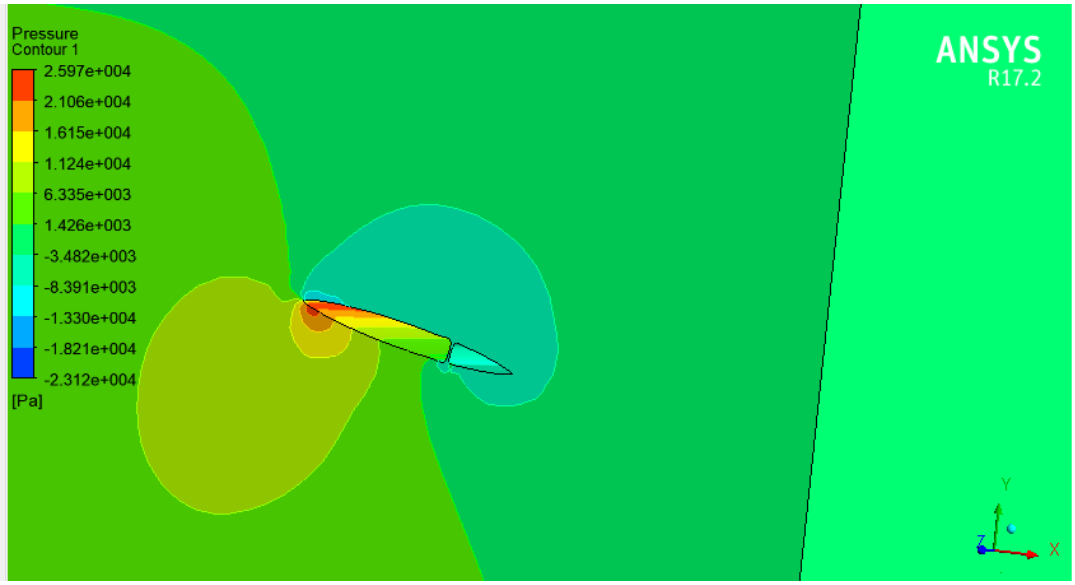

Figure 3. Pressure contour over NACA 23012 airfoil with zero flap angle and at AoA=12°.

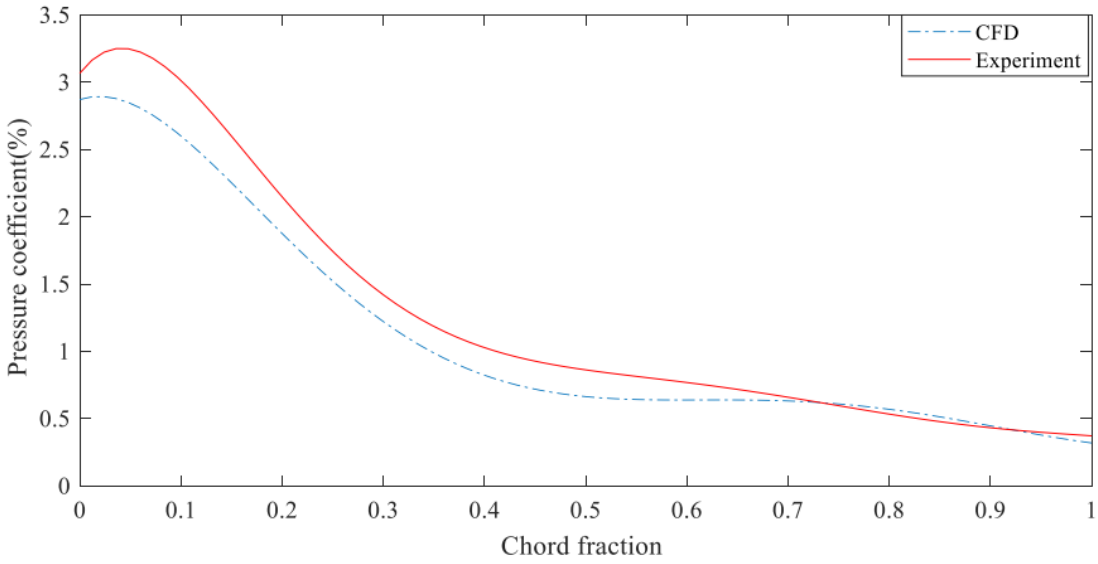

Figure 4. Experimental and CFD results for the pressure coefficient along the surface of the airfoil with zero flap deflection at AoA=12°.

RESULT AND DISCUSSION

The simulation was carried out using the Fluent software for different lengths of the flap at (Re= 6.3×10^6) under subsonic fluid flow. The contour of pressure distributed over NACA 23012 airfoil with flap angle 25°and AoA setting at 20°, was shown in Fig. 5. It is clearly seen that the high-pressure zone apparently occurs at the leading edge and the lower surface of airfoil, while the low-pressure zone happens on the upper surface of the airfoil. The velocity over the airfoil surface was induced relative to the flap produces a vortex near the trailing edge, which leads to the rise of the velocity on both the upper and the lower surfaces. The vortex is also creating a local low-pressure region, which greatly improves the pressure, accordingly with a drawback in reducing the gradient severity of the adverse pressure.

In this section, the results for various cases of the flap geometry are presented together with a final comparison. The predicting of the pressure distribution over NACA 23012 airfoil with various flap angles at setting AoA, is the main objective of each case.However, at zero AoA as shown in Fig.6, it is eventually seen that the average pressure distribution over airfoil increases relative to growth in the flap angle for all cases. The flap has produced a vortex near the trailing edge, which helps to induce a velocity over the airfoil surface that leads to a rising velocity on both the upper and the lower surface .Therefore, the average pressure over a wing was able to grow by increasing the deflection angle of the flap without changing the airfoil AoA [18].

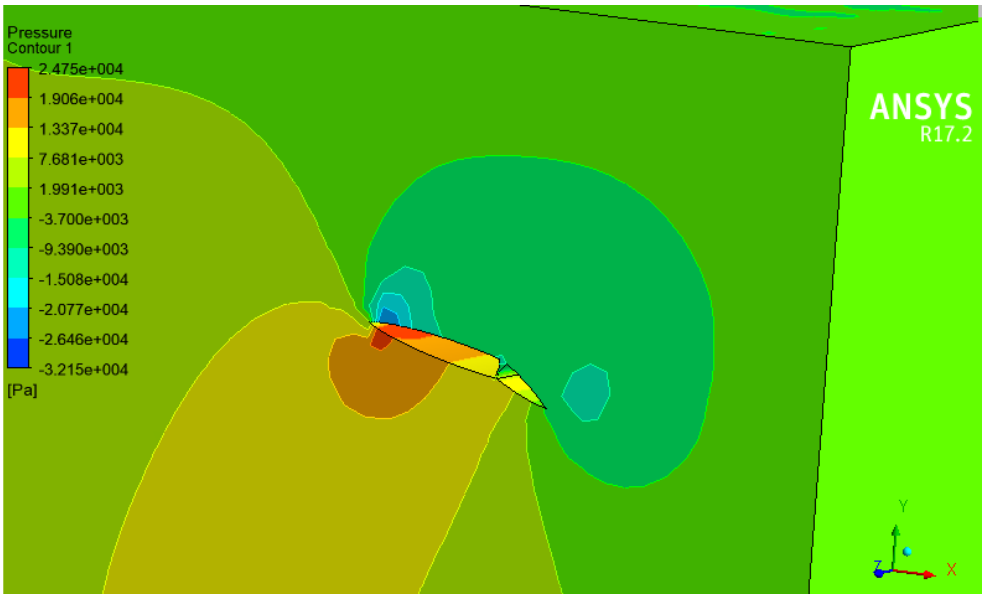

Figure 5. Pressure contour for wing with flap at Re= $6.3x10^6$and setting AoA=20°.

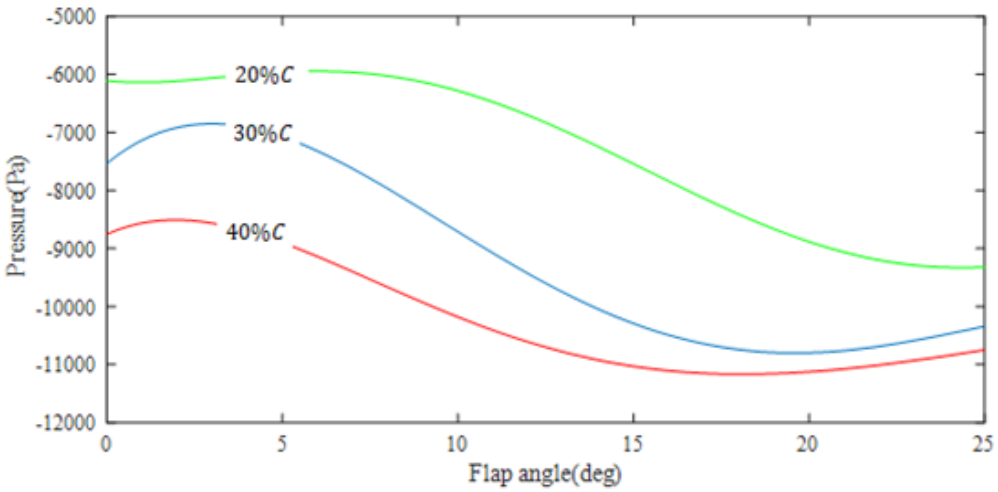

Figure 6. Pressure variation with flap deflections angle at zero AoA for different flap lengths.

By increasing the setting AoA to 10°, as shown in Fig. 7. It is observed that the average pressure is increased with a flap angle until to reach the maximum value of the pressure at the flap angle approximately equal to 10° . The flap is preventing the recirculation area from further spreading, this behavior has a feasible impact on the aerodynamic characteristics. After that, the pressure is decreasing with the increase of the flap angle due to separation flow, which was occurred at this angle with undesirable pressure gradient over the upper surface of the wing. Similarly, the same behavior was obtained at setting AoA to 20°, as shown in Fig. 8. The maximum value of average pressure was found at the flap angle approximated to 5°. After that, the average pressure is decreasing

with an increase in the flap angle. From Figs 7 and 8, it was shown that the larger increment of pressure is obtained with the larger flap chord (40 % C), and the flap length directly influences the pressure. However, with longer flaps the problem with reattachment of the flap.

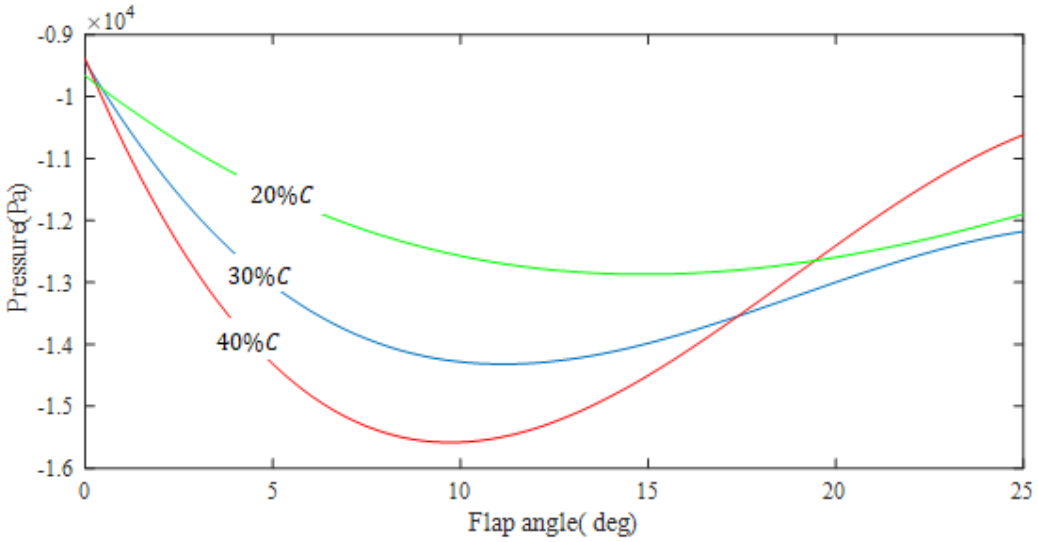

Figure 7. Pressure variation with the flap at setting AoA= 10° for different flap length.

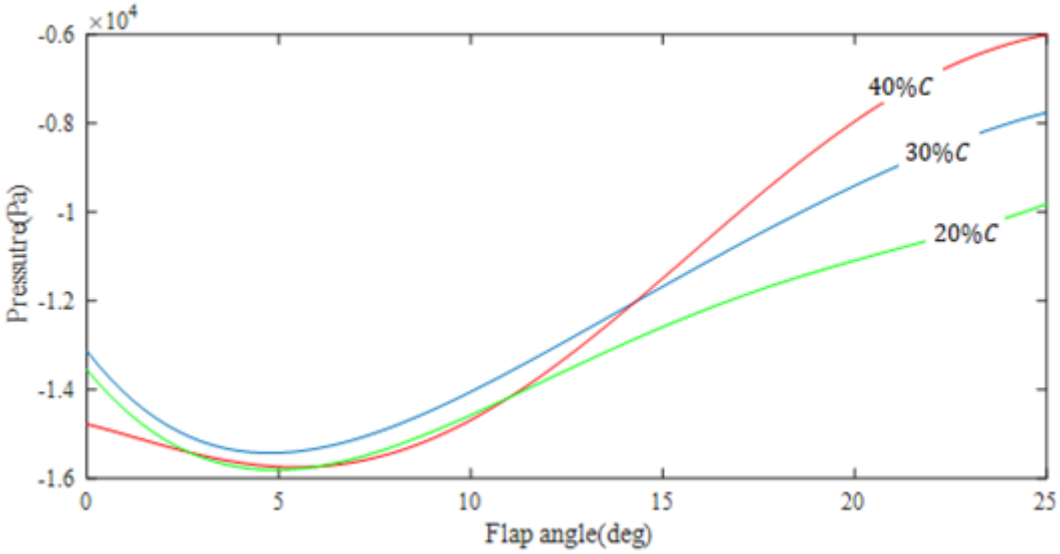

Figure 8. Pressure variation with the flap at setting AoA= 20° for different flap lengths.

The Ansys program was used to obtain the stress distribution over the wing. The preliminary design of the wing against the load is assumed from the Aluminum 7075-T651, the physical and mechanical properties of Aluminum is presented in Ref.[19]. The maximum value of stress (100.03 MPa) was found at the root of the wing relative to the maximum bending moment occurs at the root. The stress was decreased behind the root of the wing and along the length of the span until reaching the wingtip, which becomes zero. This is due to the minimum bending moment was occurred at this location as shown in Fig.9.

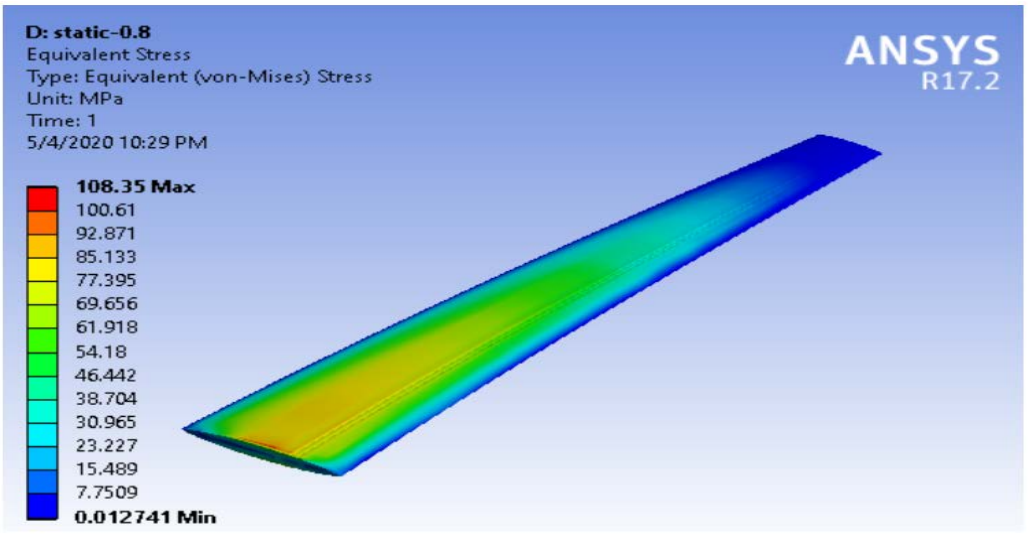

Figure 9. Stress contour for wing with flap at Re= $6.3x10^6$and zero setting of AoA.

The stress-induced over the wing structure with various flap angles for the different flap geomtry as shown in Figs. 10, 11 and 12, for setting AoA. Based on the results presented, the larger increment of equivalent stress was obtained with the larger flap chord. Also, the behaviors of the maximum stress were adapted according to the flap angle and setting of AoAs. The maximum value of stress is increased by 40 % from the other, which can be considered for design the wing structure.

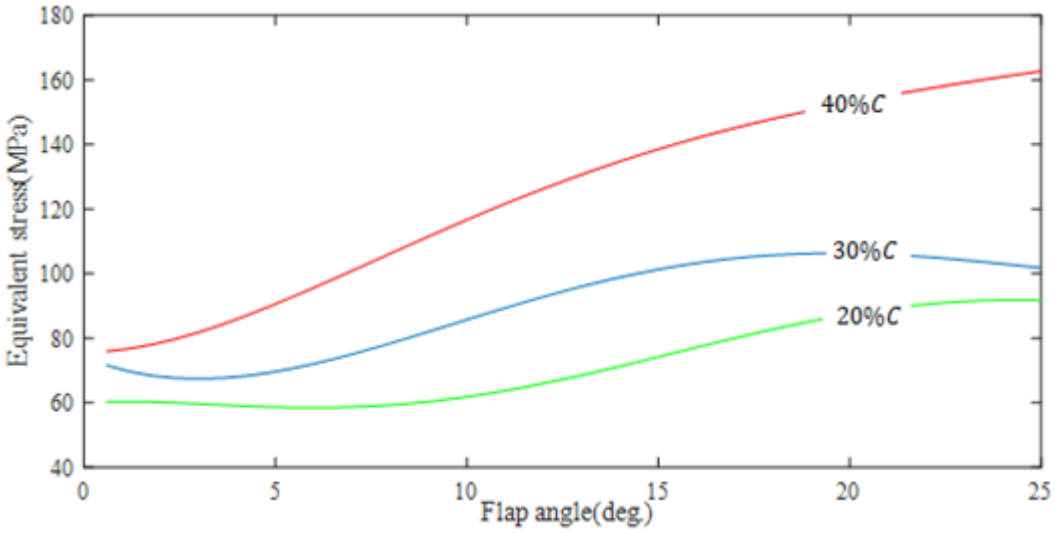

Figure 10. Stress variation with the flap deflection at zero setting of AoA for different flap lengths.

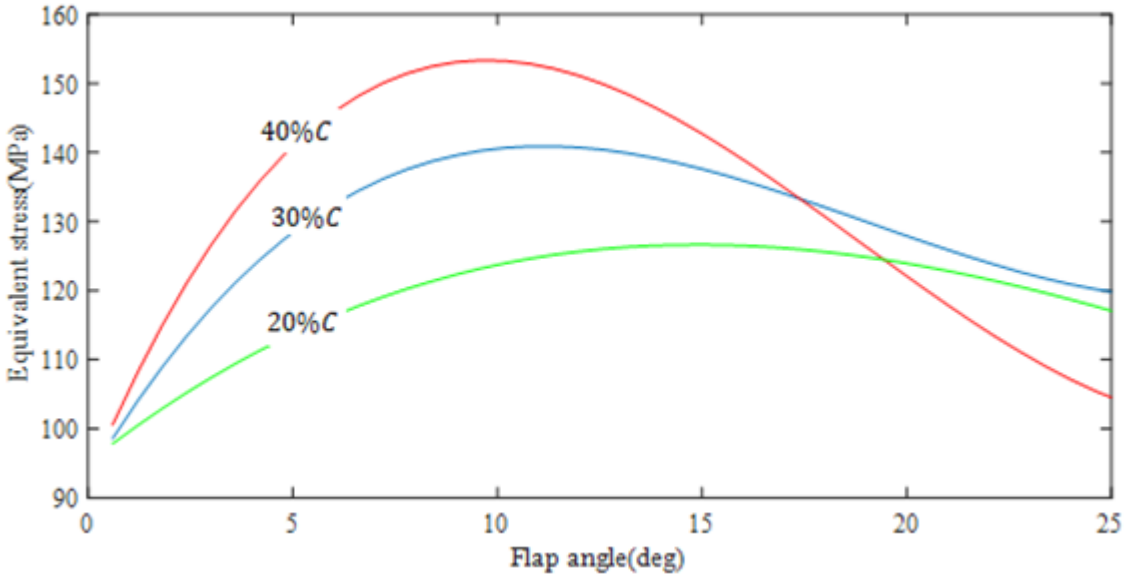

Figure 11. Stress variation with flap deflection at AoA = 10° for different flap lengths.

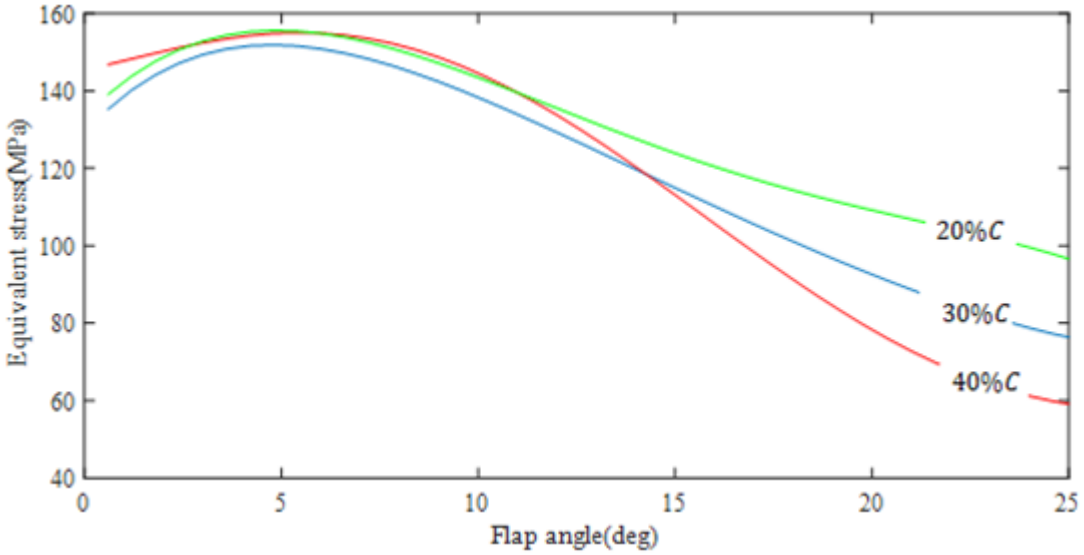

Figure 12. Stress variation with flap deflection at AoA = 20° for different flap lengths.

Figure 13 was displayed the deformation contour for wing structure with flap, the maximum deflection occurs at the free side of the tip wing at (301.35 mm). While, the wing deflection is proportional to the pressure distribution over the wing and inversely proportional to the stiffness factor EI, modulus of elasticity and second moment of area.

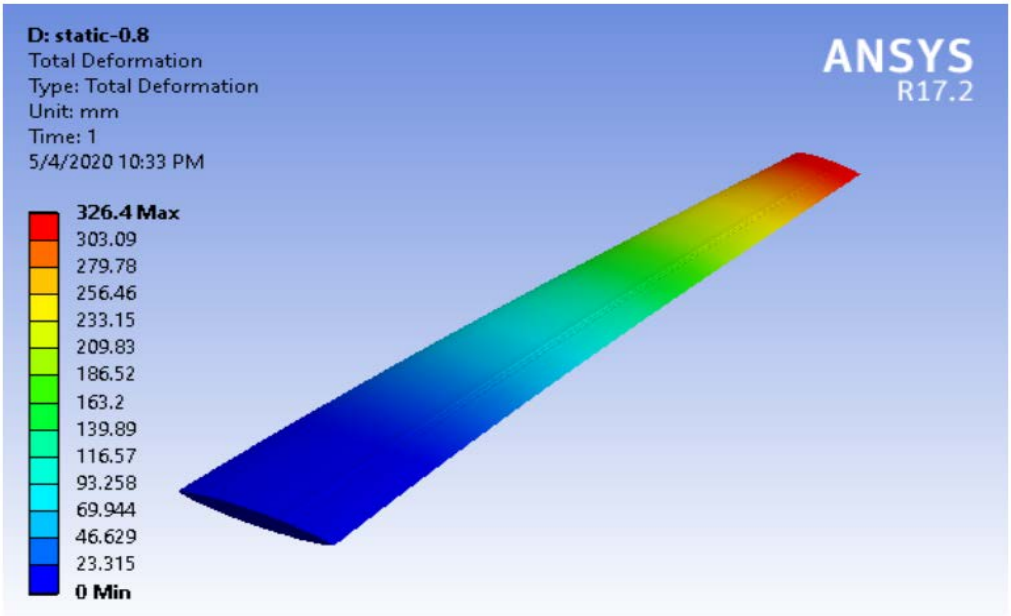

Figure 13. Deformation contour for wing with flap at Re= $6.3*10^6$and zero setting of AoA.

The total deformation of the wing structure with various flap angles for different flap geomtry as demonstrated in Figs. 14, 15 and 16, at setting AoA. It is clearly seen that the deformation was increased according to the growth of the flap deflection angle as a result of the pressure distribution over the wing. Moreover, it was found the larger increment of deformation was obtained with the larger flap chord and the maximum value of deformation is greater about 45 % of the other, the maximum deflection occurs at the free side of the wing or at the tip.

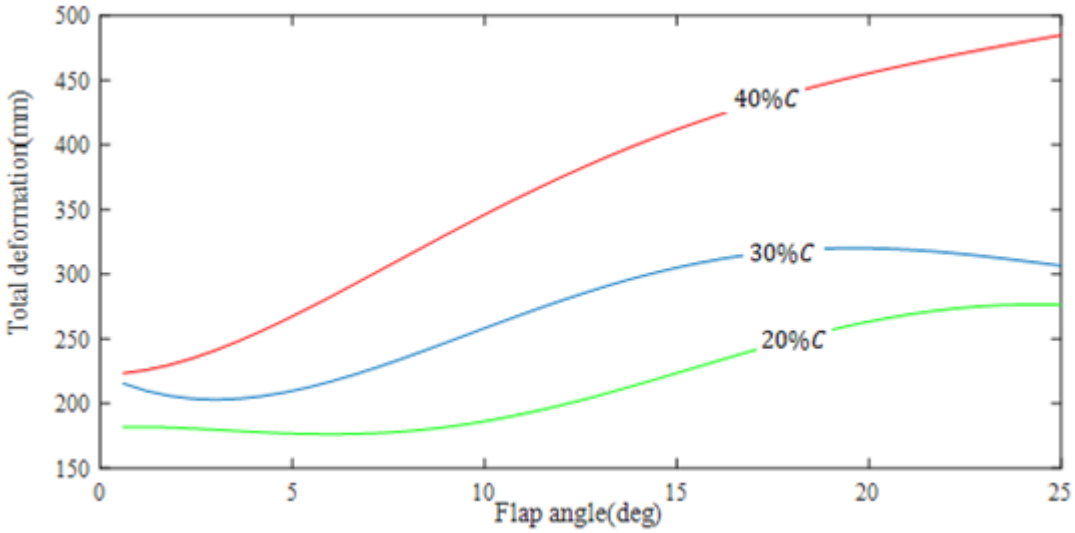

Figure 14. Deformation variation with the flap angle at zero setting of AoA for different flap lengths.

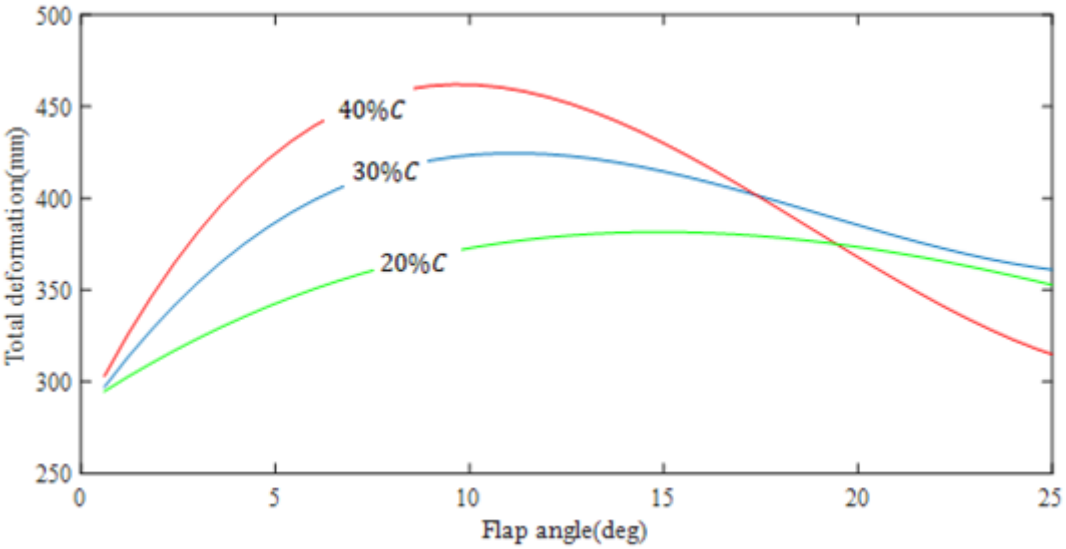

Figure 15. Deformation variation with flap deflection at AoA = 10° for different flap lengths.

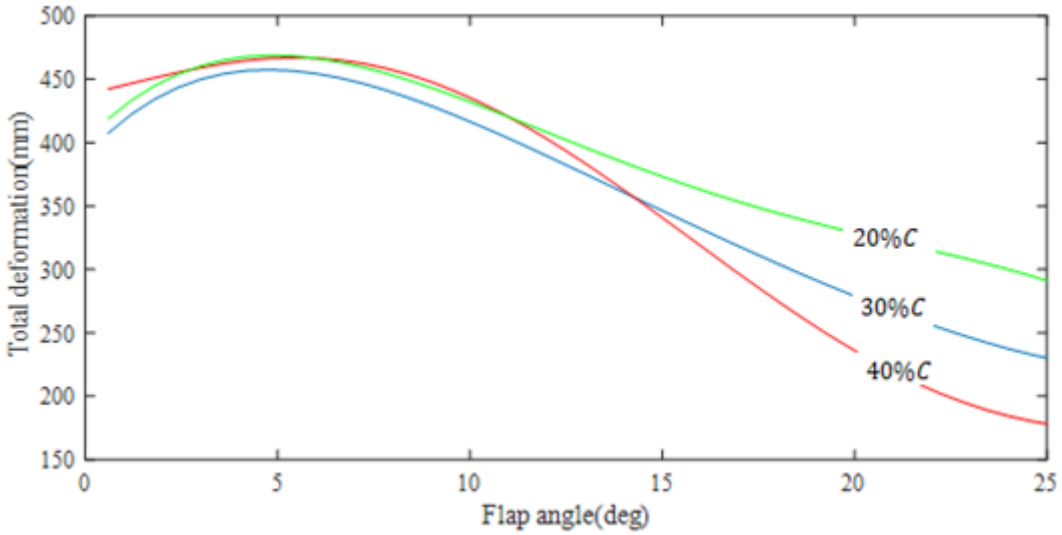

Figure 16. Deformation variation with flap deflection at AoA = 20° for different flap lengths.

CONCLUSIONS

In this work, the numerical simulations were performed in the Fluent CFD to investigate the effects of the flap geometry on the structure analysis at setting attack angle for the NACA 23012 airfoil. The dynamic mesh has been used to simulate the motion of the flap body at any position. The results will be validated by comparing with the previously published articles.

The following conclusions can be drawn from this analysis work:

1. At zero AoA, the pressure value decreases in the upper surface relative to increase the flap angle although the pressure value increase in the lower surface. When the AoA increased, the behaviors of the pressure at the upper and lower surface is varied according to the flap angle setting.
2. It was found that the maximum stress and deformation occur with the larger flap chord 40% C, corresponding to the present pressure, Thus should be considered for the wing structure design, and the highest values of stress occur at the fixed edge.
3. Depending on the results from the Fluent, it was found that the flap length 30% C has better performance and the structural efficiency compared with other lengths.

4. It is eventually seen that the average pressure distribution over airfoil increases relative to growth in the flap angle for all cases. The maximum value of average pressure was found at the flap angle approximated to 5°.
5. The maximum value of stress (100.03 MPa) was found at the root of the wing relative to the maximum bending moment occurs at the root. So, the maximum deflection occurs at the free side of the tip wing at (301.35 mm).

REFERENCES

[1] N.R. Kluga. A Study of Flap Management, an Analysis of the Consequences of Flap Management, and a Search for Possible Causes. *Journal of Aviation/Aerospace Education & Research*. 1991.

[2] J.F. Granizo, Snorri Gudmundsson, and William A. Engblom. Effect of the Slot Span on the Wing Performance. In 35th AIAA Applied Aerodynamics Conference. 2017: 3578.

[3] M. Todorov. Aerodynamic Characteristics of Airfoil with Single Slotted Flap for Light Airplane Wing. Proc. of AFASES. 2015: 509-514.

[4] N. Mahjoubi, Gravouil A, Combescure A. and Greffet N. A Monolithic Energy Conserving Method to Couple Heterogeneous Time Integrators with Incompatible Time Steps in Structural Dynamics. *Computer Methods in Applied Mechanics and Engineering*. 2011; 200(9-12):1069-1086.

[5] W.Q. Wang, Yan Y. Strongly Coupling of Partitioned Fluid–Solid Interaction Solvers Using Reduced-Order Models. *Applied mathematical Modelling*. 2010; 34(12): 3817-3830.

[6] C. Wood, Gil AJ, Hassan O, Bonet J. Partitioned Block-Gauss–Seidel coupling for Dynamic Fluid–Structure Interaction. *Computers & structures*. 2010; 88(23-24): 1367-1382.

[7] H. Dang, Yang Z, Li Y. Accelerated Loosely Coupled CFD/CSD Method for Nonlinear Static Aeroelasticity Analysis. *Aerospace Science and Technology*. 2010; 14(4): 250-258.

[8] P. Gamboa, Vale J, Lau F J P and Suleman, A. Optimization of a Morphing Wing Based on Coupled Aerodynamic and Structural Constraints. *AIAA journal*. 2009; 47(9): 2087-2104.

[9] B.S. Jianan Tan, A Study of Solving navier Stokes Equations with a Finite Volume mMethod Based on Polygonal Unstructured Grids and the Computational Analysis of Ground Vehicle Aerodynamics, PhD in Mechanical Engineering, 2010.

[10] E.Q. Hussein, Farhan Lafta Rashid, Haider Nadhom Azziz, 2019 Aerodynamic Heating Distribution for Temperature Prediction of Fast Flying Body Nose Using CFD. *Journal of Advanced Research in Fluid Mechanics and Thermal Sciences*, 64(2); pp 21-27.

[11] E.Q. Hussein, Basim Raheem Sadeq, Frarhan Lafta Rashid. "Failure Analysis of Composite Plate with Central Opening Hole Subject to Arbitrary Tension Load", *Journal of Mechanical Engineering Research and Developments*, vol.43,2020.

[12] C.P. Van Dam. The Aerodynamic Design of Multi-Element High-Lift Systems for Transport Airplanes. *Progress in Aerospace Sciences*. 2002; 38(2): 101-144.

[13] I.H. Abbott, Von Doenhoff A E. Theory of wing sections: including a summary of airfoil data. *Courier Corporation*. 2012.

[14] A. Riddle, Carruthers D, Sharpe A, McHugh C, Stocker J. Comparisons Between FLUENT and ADMS for Atmospheric Dispersion Modelling. *Atmospheric Environment*. 2004; 38(7): 1029-1038.

[15] E.F. Sheta, Harrand V J, Thompson D E, Strganac T W. Computational and Experimental Investigation of Limit cycle Oscillations of Nonlinear Aaeroelastic Systems. *Journal of Aircraft*. 2002; 39(1): 133-141.

[16] T.A. Harris, Lowry J G. Pressure Distribution Over an NACA 23021 Airfoil with a Slotted and a Split Flap. *US Government Printing Office*. 1941.

[17] T.A. Harris, John G L. Pressure Distribution Over an NACA 23021 Airfoil with a Slotted and a Split Flap. *US Government Printing Office*. 1941.

[18] E.Q. Hussein, Haider Nadhom Azziz, Farhan Lafta Rashid, "Aerodynamic Study of Slotted Flap for NACA 24012 Airfoil by Dynamic Mesh Techniques and Visualization Flow", *Journal of Thermal Engineering*, Vol. 7, No. 2, Special Issue 13 pp. 230-239, February, 2021.

[19] T. Azimzadegan, Serajzadeh, S. An investigation into microstructures and mechanical properties of AA7075-T6 during friction stir welding at relatively high rotational speeds. *Journal of Materials Engineering and Performance*, 19, 1256–63, 2010.